Build Simul (2020) 13: 1305–1319
https://doi.org/10.1007/s12273-020-0634-1

# Experimental and numerical study of the airflow and thermal characteristic of non-uniform transpired solar collector

**Dengjia Wang[1,2] (✉), Meng Gao[2], Qian Gao[2], Yanfeng Liu[1,2], Yuan Liu[2], Jiaping Liu[1]**

*1. State Key Laboratory of Green Building in Western China, Xi'an University of Architecture and Technology, Xi'an 710055, China*
*2. School of Environmental and Municipal Engineering, Xi'an University of Architecture and Technology, Xi'an 710055, China*

## Abstract

A transpired solar-collector is a device, which is attached to building walls, that uses solar energy to provide preheated fresh outdoor-air before it is drawn into the building through the ventilation system. A transpired collector consists of a heat-collection plate with infiltration holes, an air layer, an air outlet, and other auxiliary components. A transpired solar collector with non-uniform holes is investigated in this paper, and a physical model for it is developed. The model is then simplified to enable effective simulation and subsequently verified by experiments to evaluate the reliability of the simulation results. Furthermore, a multi-factor sensitivity analysis of a transpired solar collector, with respect to airflow and thermal characteristics, is performed using a numerical simulation. In addition, the application of the device is combined with the thermal requirements of the actual building. The results show that the air-layer thickness has the strongest effect on the heat-collection efficiency, which can be increased to 93% when thickness is 30 mm and height ratio is 0.30. This effect is obvious only in the case of non-uniform perforation. Although a high air-velocity can increase the daily heat-exchange by 595.2 W, the average daily air-supply temperature decreases by 34.2 °C. Even though the temperature-target may not be reached when more fresh air is introduced, the reduction of the fresh air heating-load is substantial.

## Keywords

non-uniform transpired solar collector,
airflow and thermal characteristics,
experiment,
numerical simulation

## Article History

Received: 21 October 2019
Revised: 02 March 2020
Accepted: 07 March 2020



## 1 Introduction

The energy consumption and environmental problems related to heating and cooling of buildings are big and increasing problem in many countries (Zhang 2008). As a result, the search for renewable energy solutions continues. Solar energy has been studied extensively with regard to heating and radiant cooling in the building construction sector (Sameti and Kasaeian 2015; Liu et al. 2018). Currently, among the many passive technologies that use solar heating (Liu and Li 2015) (e.g. direct-gain type), attached sunrooms and solar walls are the most promising thanks to their simplicity and low implementation-cost. The solar wall, specifically, is favored by many researchers because of its big potential for better architectural integration and versatility.

There have been many studies of solar walls for heat collection and heat storage. For example, the Trombe wall, designed by French scientist Felix Trombe, was built in Odysseus in 1967 (Torcellini and Pless 2004; Safer et al. 2005; Chen 2010). The research of this kind of solar wall mainly focused on the different types of venetian-blind-base designs (He et al. 2016; Chen et al. 2016), heat-pipe solar walls (Zhang et al. 2006), and lattice solar walls (Wang et al. 2013). In addition to related improvement- and extension-research, Liu et al. (2018) used phase-change materials at different locations in the new ventilated Trombe wall. This improved the thermal performance of the wall, alleviated overheating-problems during the day, and increased the heat-storage capabilities at night. Helenice et al. (2011) combined the Trombe wall with glass to improve the curtain wall system performance. The results show that a Trombe wall, with double self-cleaning glass, can reduce the energy consumption significantly. Choudhary et al. (2008) described the design and analysis that the Georgia tech solar decathlon team conducted for an 800-square-foot solar house in 2007. Thanks to this project, the process could be used for final

E-mail: wangdengjia@xauat.edu.cn

testing and fine-tuning of building components on site, as well as for optimized control of the energy management, when the house was fully operational. The results indicate that these solar walls can effectively increase the indoor temperature and reduce the heating load in winter. However, these wall structures are of the internal circulation type, and it is difficult to take into account any improvements in indoor air quality during winter.

Therefore, transpired solar collectors (TSCs) were proposed, which consist of a heat-collection system and an airflow facilitation system. The heat-collection system consists of an infiltration heat-collection plate, air layer, infiltration holes, and other auxiliary components. The air-layer absorbs the radiant heat of the heat-collection plate via thermal convection to preheat fresh air coming from outside. Because of the large dynamic pressure but small static pressure at the small hole, the pressure difference, which is generated by the suction of the small hole, adsorbs the air at the heat collecting plate. This facilitates convective heat-transfer. Furthermore, convective heat-loss is small because of the continuous absorption at the convective boundary layer and the infiltration holes. Such systems were first implemented by companies like Conserval, in Canada, or Cardiff university in the UK (Saxena et al. 2015).

Later, many researchers studied these systems considering operating parameters, structural parameters, and environmental parameters. With regard to operating parameters, Belusko et al. (2008), for example, used jet impingement in a porous solar-wall and found that a jet shock can increase the thermal efficiency of the collector by 21%. Collins and Abulkhair (2014) used numerical models to verify the experimental results and analyzed a set of different suction-speeds, the effect of thermal efficiency and evaluation of the heat transfer, and effectiveness of the collector plate. Chan et al. (2013, 2014), performing an analysis of two-way air flow, found that, when the air temperature in the cavity is uneven, vertical flow plays can increase the airflow temperature by 40%, which means the heat exchange between the back of the board and the air cannot be ignored. By comparing a flat solar wall with a permeable solar wall, it was found that the permeable solar wall can reduce heat-loss, and its thermal efficiency can be 50% higher than a flat solar wall (Li et al. 2013; Gao et al. 2020).

Many researchers focused on the structural parameters of the collector plate. Motahar (2010) used a steady-state model to analyze the effect of pore diameter, pore spacing, and seepage velocity on exergy efficiency. Njomo (2000) analyzed the overall heat-exchange of the solar wall using a mathematical model and studied the effect of air-inlet temperature, mass flow, and air-cavity thickness on the heat-collection performance of the heat-collection plate. Gholampour and Ameri (2014) proposed a similar mathematical model to study the energy and effective energy of porous solar-walls. Gawlik et al. (2005) determined the performance of a porous solar wall with low thermal conductivity via a numerical simulation and experiments. The results showed there was little difference between the equivalent geometric shapes of materials with low thermal-conductivity and those with high thermal-conductivity. Croitoru et al. (2016) analyzed the effect of the shape of the permeability hole on the heat transfer. The group found that the flow of the leaf-shaped permeability hole was more complex than for the circular hole, which exhibited better heat-transfer. van Decker et al. (2001) studied the heat-exchange efficiency with different hole shapes based on Kutscher's study. Red and Ameri (2016) analyzed the energy and exergy efficiency of the two-stage porous solar wall using a mathematical model and verified it with experimental results.

Studies show that environmental parameters such as solar radiation intensity and air speed also affect the thermal performance of the porous solar wall. Kutscher et al. (1993) proved that, for porous solar walls, when the outdoor air-velocity and the suction velocity of fresh air are within a certain range, the heat loss due to natural convection is small, while the majority of the heat loss is the radiation. Dymond and Kutscher (1995) set the porous plate as the boundary condition for a continuous fluid. They carried out an overall CFD simulation of the solar wall and obtained the temperature and pressure of the air at the outlet of the air layer. Wang (2009) analyzed the effect of solar-radiation intensity, outdoor air-speed and outdoor air-temperature on the thermal performance of a solar-wall system, both experimentally and theoretically. Some scholars have studied the airflow characteristics of the solar chimney channel. For example, Li et al. (2007) put forward the mathematical model for a solar chimney and verified the correctness of the model through experiments. The performance of the glass solar chimney was affected by channel width and solar thermal gain. Hong et al. (2019) studied the effect of the solar chimney on the annual ventilation of buildings. The results indicate that the system could reduce the annual ventilation by 77.8% and the annual VRF ventilation by 2.3%.

However, research of the TSCs above mainly focused on the uniform distribution of infiltration holes, and seldom considers the short-circuit problem caused by the non-uniform distribution of infiltration holes under the action of thermal- and air-pressure. By analyzing both the air distribution and path line of the TSC, it was found that the first heat-transfer occurred when air came into contact with the outer surface of the plate. The second heat-transfer, on the other hand, occurred at the inner surface of the plate,

when the air reached the air layer. As a result, no secondary heat-transfer takes place for the air reaching the air layer through the holes near the fan. This could be used to increase the thermal efficiency of the TSC. For these reasons, a non-uniform opening is studied in this paper, which allows altering the flow pattern and increase the second heat-transfer.

In this paper, the flow and thermal properties in the flow channel of the TSC were analyzed via numerical simulation for different suction speeds, hole-sizes and -distributions, and air-layer thicknesses. The effect of several parameters on the thermal properties and flow of the TSC were obtained in a flow channel. In addition, the TSC heat-gain, for different ventilation rates, was compared with the building's fresh air heating-load. This was done to determine the reduction effect of the TSC on the building's fresh air heating-load.

## 2 Methodology

### 2.1 Description of a non-uniform transpired solar-collector

A transpired solar-collector is typically used to penetrate the outside air and increase the heat boundary to reduce heat loss. This is caused by infiltration holes in the heat collection plate. However, due to the suction effect of the fan at the outlet, the small holes near the fan are short-circuited by the higher air-pressure, which resulted in a partial airflow. Therefore, it was impossible to perform a full heat exchange with the heat-collection plate, and the thermal efficiency decreased. In order to solve this problem, a non-uniform opening for the heat-collection plate was investigated. Figure 1 shows that the non-uniform opening of the collection plate could cause the short-circuit flow develop completely unlike the one with the uniform opening. The non-uniform opening leads to larger heat-loss at the non-porous plate surface. Therefore, the difference between heat loss and heat gain is mainly reflected in the proportion of the non-uniform opening. In this paper, the sensitivity of the TSC with non-uniform perforation was analyzed to determine the ratio for non-uniform perforation, in other words, the height ratio $H^*$. Figure 2 shows the three types of non-uniform-orifice collection plates. Here, $H^*$ is the ratio of the opening height, ordered from top to bottom of the infiltration holes, to the overall height of the heat-collection plate assuming that both row spacing and column spacing remain unchanged (at 10 cm). Sunlight hit the heat-collection plate and increased the temperature. The fresh air from the outside reached the air layer through the holes, and the air in the air layer exchanged heat with the heat collector. It then entered the room through the air outlet due to air- and thermal-pressure.

### 2.2 Theoretical analysis

#### 2.2.1 *Analysis of thermal efficiency of the system*

The thermal efficiency of the system is mainly determined by the heat exchange efficiency and the heat-collection efficiency (Wang et al. 2019). Heat exchange efficiency and heat-collection efficiency are important for a TSC and reflect the capacity of air to absorb heat from the heat-collection plate and to absorb the total radiant heat.

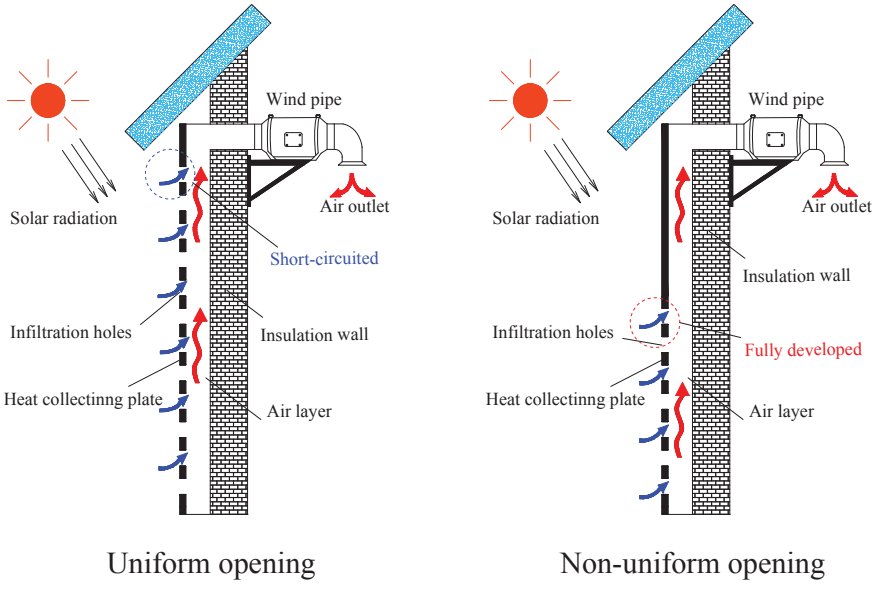


**Fig. 1** Schematic of a non-uniform transpired solar collector

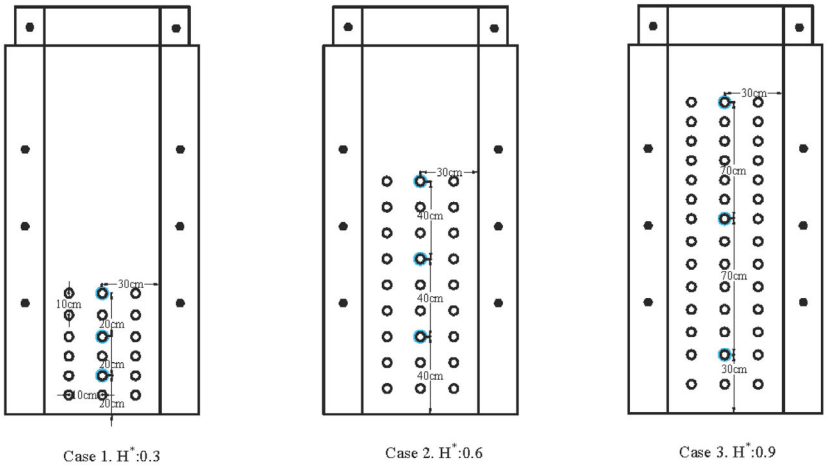


**Fig. 2** Schematic of a non-uniform heat-collection plate

The heat-exchange efficiency $H_\varepsilon$ is the ratio of the actual temperature difference in the system to the theoretical maximum temperature-difference:

$$H_\varepsilon = \frac{T(\tau)_{out} - T(\tau)_{in}}{T(\tau)_p - T(\tau)_{in}} \quad (1)$$

where, $T(\tau)_{in}$ is the average temperature of the environment; $T(\tau)_{out}$ is the average outlet-temperature; $T(\tau)_p$ is the average temperature on the surface of the heat-collection plate.

The heat-collection efficiency $\eta$ is the ratio of the total heat absorbed by air through the collector plate to the solar radiation:

$$\eta = \frac{m(\tau)c_a\left[T(\tau)_{out} - T(\tau)_{in}\right]}{IA} \quad (2)$$

where, $c_a$ is the specific heat-capacity of the heated air; $I$ is the solar radiation intensity; $A$ is the area of the collection plate exposed to solar radiation; $m(\tau)$ is the air-mass flow through the system, which is calculated as follows:

$$m(\tau) = A_{ph} v_{ph} \rho_{ph} \quad (3)$$

where, $A_{ph}$ is the cross-sectional area of infiltration holes; $\rho_{ph}$ is the air density of the infiltration hole; $v_{ph}$ is the air speed through the infiltration hole.

### 2.2.2 *Analysis of the heating load*

The purpose of the TSC was to preheat the fresh air, thus, only the heating load, which was carried by fresh air streaming into the building, was considered in this paper. To study the elimination effect of a TSC on the fresh air heating-load, it is necessary to calculate the load for the building. The building's fresh air heating-load was calculated using the following equation:

$$Q = 0.278 C_p V \rho_w \cdot (t_n - t_w) \quad (4)$$

where, the source of 0.278 is the unit conversion factor, i.e., 1 kJ/h= 0.278 W. $C_p$ is the constant-pressure mass-specific heat-capacity of dry air, i.e., 1.0056 kJ/(kg·°C); $\rho_w$ is the air density at outdoor heating temperature in kg/m$^3$; $V$ is the cold-air infiltration volume flow in the room in m$^3$/h; $t_n$ and $t_w$ are the indoor- and outdoor-heating calculation temperatures, respectively.

## 2.3 Numerical simulation

### 2.3.1 *Modeling and boundary conditions*

A high-resolution computational domain has been created to reproduce the physical TSC system. This was done to capture the multi-scale fluid-flow properties across a perforated plate and within the perforations as well as the jet flow that emerge from them. The model size of the transpired solar collector (length × width × height) was 0.6 m × 0.05 m × 2.1 m, with a hollow structure. The interior consisted of an airflow channel. The boundary types and settings are shown in Table 1**.** The heat-collection plate is made of a non-transparent material, which cannot be loaded with solar radiation terms using the Fluent simulation software. Therefore, the user-defined function, UDF, was used to fit the outdoor solar-radiation of a typical city in western China on a typical day (January 23, the day with the smallest average temperature-difference was the coldest outdoor month), see Figure 3. Considering that the absorptivity of the collection plate (experimentally determined as 0.92), we multiplied the corresponding coefficient and wrote the function such that the heat flow term loaded on the collecting plate was obtained.

The convective heat-transfer coefficient of the air-outlet pipe was $h$ = 5.7+3.8 × $v$, where $v$ is the wind speed. Using the meteorological parameters of "*the Practical Air Conditioning*

**Table 1** Boundary types and settings

| Types | Boundary settings |
|---|---|
| Heat-collection plate | Neumann boundary condition<br>Heat-flux boundary |
| The wind pipe | Third boundary condition<br>Convection and radiation-mixing boundary |
| Insulation wall | Neumann boundary condition<br>Adiabatic boundary |
| Air outlet | Velocity outlet condition<br>Variable air velocity |
| Infiltration hole | Pressure inlet condition<br>Default parameters |

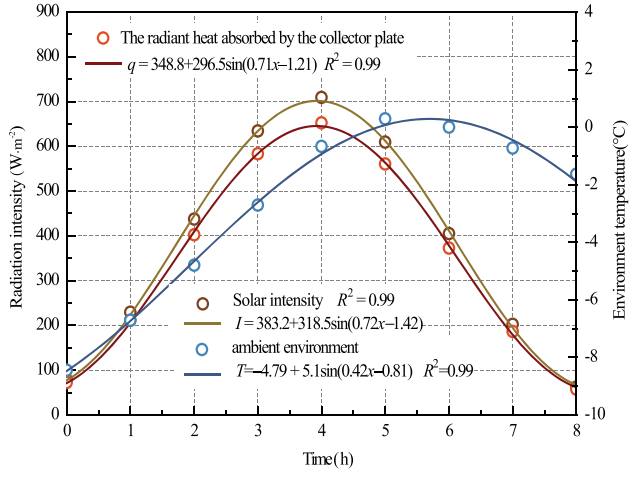


**Fig. 3** Radiation intensity and ambient temperature for a typical diurnal climate and environment in winter

*Heating Design Manual*" (Lu 2008), the average outdoor wind-speed was 2 m/s in winter, while the indoor wind-speed was 0.3 m/s near the air-outlet pipe. The convective heat-transfer coefficients were 13.3 W/(m²·K) and 6.84 W/(m²·K), respectively. The air temperature parameters were selected and the city's meteorological parameters were fitted, see Figure 3. In addition, the user-defined function, UDF, was prepared. Considering that the wall was equipped with insulation material, it was set as adiabatic boundary condition to simplify the calculation. Due to the suction action of the fan, with constant wind-speed, it was defined as the boundary condition for the velocity outlet, and different suction wind speeds were set considering varying suction action. The infiltration inlet was defined as a pressure inlet, and the initial parameters remained at their default values.

The commercial CFD software ANSYS Fluent (version 16.0) was used to solve the three-dimensional non-steady-state conservation equations for mass, momentum, and energy. GAMBIT 2.4.6 was used for all geometric models, and ICEM (version 16.0) was used for the mesh generation. The Mesh Size was 0.01 m, and the Mesh Quality was the result of automatic checks in Fluent 16.0, which showed Minimum Orthogonal Quality = 0.667 (this value ranges from 0 to 1; the closer it is to 0, the lower is the Quality), and Maximum Ortho Skew = 0.331 (this value ranges from 0 to 1; the closer it is to 0 the higher is the Quality).

### *2.3.2 Determination of the meteorological parameters and radiation model*

The climatic and environmental parameters for typical winter days in western China were obtained via data investigation (Liu et al. 2020), the results of the nonlinear fits are shown in Figure 3. The $x$-coordinate represents the eight hours from 10:00 to 18:00. It can be seen that the solar radiation hitting the south wall of the building was the highest around 14:00. The function in this figure was inserted into the ANSYS Fluent software as climate parameter, and all simulations were run using this parameter. Considering the mutual radiation between the high-temperature inner walls of the air chamber, the DO radiation model was set. In addition, the solar radiation intensity was compiled from meteorological parameters and plugged into the radiation model.

### *2.3.3 Turbulence model*

For a constant air speed study, the Reynolds number of air for forced flow was calculated, and the appropriate turbulence model was selected according to the degree of turbulent flow. According to the calculation results, the Reynolds number for air is greater than 4000 for a completely turbulent flow field. Thus, the calculation model used the standard $k$-$\varepsilon$ two-equation model. The Boussineq approximation was used, in consideration of the air-density-change caused by temperature change under the action of thermal pressure in the airflow channel.

Taking into account the recommended value by Launder for the experimental verification, the values of the empirical constants $C_{1\varepsilon}$, $C_{2\varepsilon}$, $C_{3\varepsilon}$, $\sigma_k$, $\sigma_\varepsilon$ and $C_\mu$ were, respectively, as follows:

$$C_{1\varepsilon} = 1.44,\ C_{2\varepsilon} = 1.92,\ C_{3\varepsilon} = 1,\ C_\mu = 0.09,\ \sigma_k = 1.0,\ \sigma_\varepsilon = 1.3$$

The $k$ equation considers the buoyancy automatically for the $G_b$ item. To consider the buoyancy effect in the $\varepsilon$ equation, the full buoyancy effect options were selected in the viscous model panel. Because the default $G_b$ is zero in the equation, the effect of buoyancy can be ignored.

### *2.3.4 The solution algorithm*

To enhance the stability of the TSC system simulation, the numerical method for the discrete pressure equation used PRESTO!. Because the computation required additional stability and computational efficiency, the SIMPLEC algorithm was adopted for iterative solution-finding and the

default Under-Relaxation Factors were kept. The accuracy of the unsteady state simulation was determined based on the degree of spatial dispersion of the fluid flux. Therefore, in order to improve the calculation accuracy, the momentum- and energy-equations used the second-order airward scheme. The remaining options were in a first-order upwind format.

#### 2.3.5 *Simulation conditions*

The used simulation conditions are shown in Table 2. The hole diameter refers to the diameter of the permeable hole in the heat-collection plate. The parameter $H^*$ is the ratio of the height of the infiltration hole to the height of the heat-collection plate, which reflects the unevenness of the opening. The suction speed of the fan refers to the air speed through the fan when the fan was running. The air-layer thickness is the thickness of the air-heating layer between the heat-collection plate and the outer wall of the building in the TSC system. At the beginning, the simulated time step was adaptive to the model. A fixed time-step of 60 s was used after the calculation became stable, and the iteration was set to 1000 times for each step. After iteration convergence, the next iteration was automatically carried out, and the number of steps was set to 540 according to the running time.

**Table 2** Infiltration-hole diameters, height ratios, fan suction speeds and solar radiation intensities for different operating conditions

| Hole diameters $D$ (mm) | Height ratios $H^*$ | Fan suction speeds $v_s$ (m/s) | Air-layer thickness $\delta$ (mm) |
|---|---|---|---|
| 2 | 0.15 | 0.325 | 30 |
| 3 | 0.3 | 0.525 | 50 |
| 4 | 0.45 | 0.725 | 70 |
| 5 | 0.6 | 0.925 | 90 |
| 6 | 0.75 | 1.125 | 110 |
| — | 0.9 | 1.325 | 130 |

### 2.4 Experimental setup

The experiment was performed to verify the simulation results. The light source used in the experiment was a TRM-PD1 matrix simulation light-source for solar simulation (i.e. an artificial sun). The heat-collection plate was 80 cm away from the solar simulator. The heat-collection plate was made of the metal plate and measured 1.9 m × 0.6 m × 0.0015 m. The surface was painted with black paint and has different numbers of perforations, holes, and rows. The distance was 10 cm; the size of the insulation wall was 1 m × 2.3 m × 0.12 m, which was filled with a double-sided 4.26 mm thick colored steel plate and a 120 mm thick polyurethane plate; 5 cm gap existed between the heat-collection plate and the thermal insulation wall. The air chamber was sealed and the air could only enter the cavity through the infiltration hole; the air chamber has a vent at the top, and the air-outlet diameter was 150 mm. The power unit used in the experiment is an HF-150PZP type axial flow fan (adjustable air-speed), the power was 44–54 W. Photographs of the heat-collection plate and the setup are shown in Figure 4. The above experiment was used to verify the simulation results. The verification conditions are shown in Table 3.

## 3 Experimental results

### 3.1 Heat-flux density

The average heat flux variation of the heat-collection plate and wall for different positions are shown in Figure 5. The

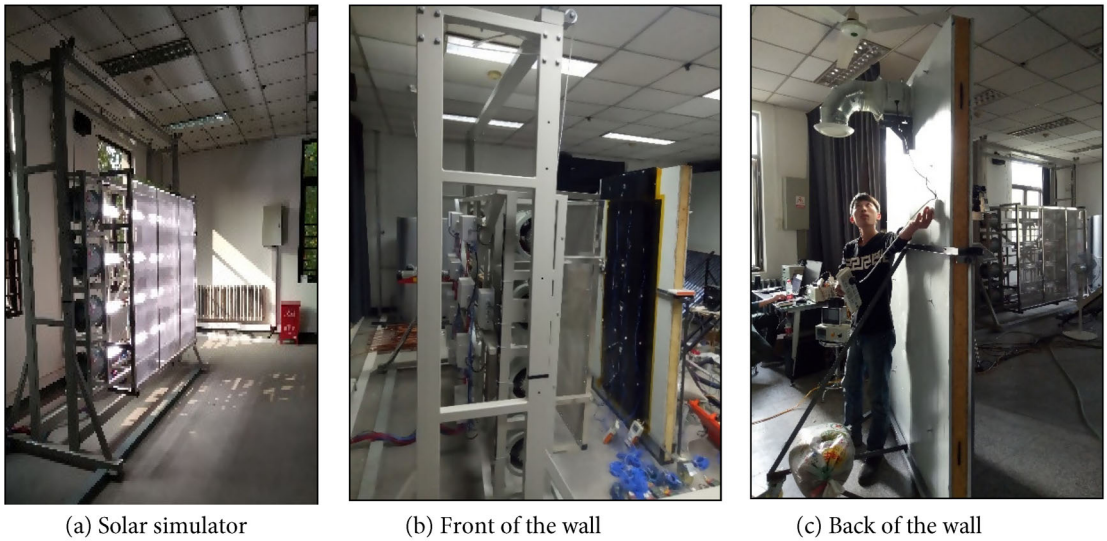

(a) Solar simulator (b) Front of the wall (c) Back of the wall

**Fig. 4** Photographs of the heat-collection plate and experimental setup

**Table 3** Details of the scenarios used for the validation

| Case number | Ambient air temperature (°C) | Solar radiation intensities $I$ (W/m$^2$) | Fun suction speeds $v_s$ (m/s) | Hole diameter $D$ (mm) | Height ratio $H^*$ |
|---|---|---|---|---|---|
| 1 | 24.0 | 700 | 0.525 | 4 | 0.6 |
| 2 | 25.0 | 600 | 0.525 | 4 | 0.6 |
| 3 | 22.4 | 600 | 0.525 | 2 | 0.6 |
| 4 | 20.1 | 700 | 0.525 | 2 | 0.3 |
| 5 | 22.7 | 600 | 0.525 | 2 | 0.3 |
| 6 | 24.2 | 500 | 0.525 | 2 | 0.3 |
| 7 | 16.3 | 600 | 0.725 | 4 | 0.3 |
| 8 | 22.0 | 700 | 0.525 | 2 | 0.9 |
| 9 | 23.2 | 600 | 0.525 | 2 | 0.9 |
| 10 | 22.1 | 700 | 0.525 | 6 | 0.6 |

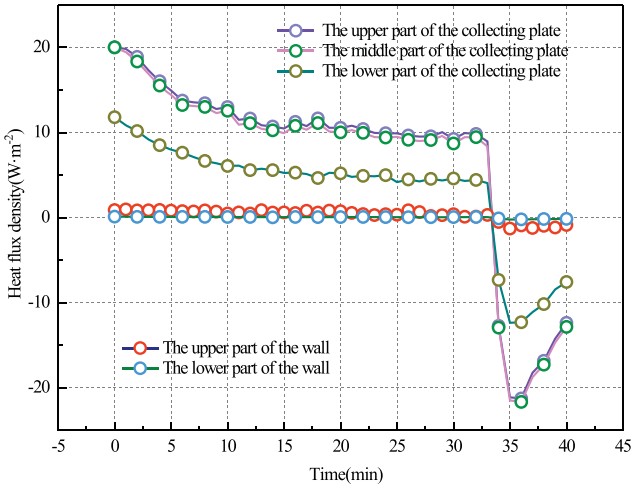


**Fig. 5** Heat flux densities, at different positions, as a function of time

figure shows that the heat exchange between the air under the collection plate and the plate was relatively small. This was due to the fact that there were dense holes below, and the mass flow during air infiltration lowered the temperature of the collection plate. As a result, the temperature difference between the heat-collection plate and the environment was lower, and the heat exchange was also lower. In addition, the low heat-flux on the wall indicates that the heat loss was low, and the heat flux decreased with time. This is due to the gradual reduction of the heat-exchange temperature-difference. After about 33 minutes, the temperature difference between the surface of the heat-collection plate and the solar simulator was even less than between the surface of the heat-collection plate and the environment. At this point, the heat flow was reversed, i.e., the direction of the heat transfer was then aiming away from the surface of the collection plate (to the environment). After 36 min operation, the heat flux density decreased gradually.

## 3.2 Infiltration-air velocity

Infiltration-air velocity refers to the flow of air in the air layer, which correlates with heat trapping. A sudden increase in the local resistance at the orifice leads to a sharp increase in the infiltration velocity, when the static pressure is converted into dynamic pressure. Porosity and infiltration-velocity are negatively correlated. Figure 6 shows that the distribution of the infiltration air speed was high in the upper and lower sections of the infiltration holes but low around the center. Due to the large number of infiltration holes in the lower part, and the high thermal upward pressure and normal air pressure, the infiltration-air velocity was high. Since the air in the upper part of the infiltration holes was close to the outlet, the high air-pressure primarily determined the infiltration velocity. As a result, the overall infiltration velocity was high. The air in the middle of the infiltration holes was subjected to low thermal and air pressure. Hence, the central part of the infiltration holes

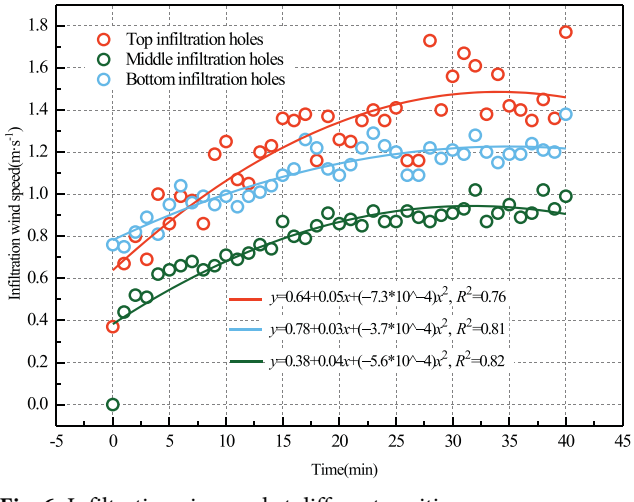


**Fig. 6** Infiltration air-speed at different positions

experienced only weak suction and the lowest infiltration air velocity.

### 3.3 Model validation

A comprehensive and functionable TSC test setup was built indoors to verify the CFD model. The experiment was carried out in a steady-state controlled indoor-environment. The solar radiation, indoor temperature and other conditions in the experiment were also constant. In order to achieve the consistency between simulation conditions and experimental conditions, steady-state simulation was selected for verification. In addition, realistic environmental conditions were selected to enable the reliable validation, see Table 3. The temperatures of the heat-collection plate, air outlet, and air layer, were verified. The results in Figure 7 show that the relative error of the numerical calculation and experimental results of outlet temperature, heat-collection plate temperature and air-layer temperature were within 10%. To simplify the calculation, it was taken into account that there is a certain difference between the calculated results and the measured results due to the difference in ambient temperature and material properties. In the experiment, the indoor temperature increased due to the solar simulator, while the ambient temperature remained constant during the simulation. In addition, because the manufacturer did not provide detailed physical parameters, the physical parameters of the materials used in the experiment differed from the simulation settings. However, the corresponding errors did not exceed 10%, which means the simulation was sufficiently accurate.

## 4 Simulation results

### 4.1 Simulated contour plots

The simulated contour plots of the air temperature within the air layer at different times are shown in Figure 8. The air layer temperature increased from morning to noon but decreased in the afternoon. The temperature gradient of the air layer increased from the bottom to the top because both the direction of the air pressure and the thermal pressure was pointing upward. The air-supply temperature at 11:00 was about 35 °C, which was suitable. At 12:00, the air supply temperature exceeded 50 °C, which causes overheating. This was counterproductive for the construction of the indoor environment, which could be cooled using phase-change materials or water coolers. At 17:00, the temperature of the air layer was generally below 15 °C. At this time, the fan should be stopped so that the air can reach the air layer through the holes via natural convection and generate thermal air resistance i.e. a thermal insulation

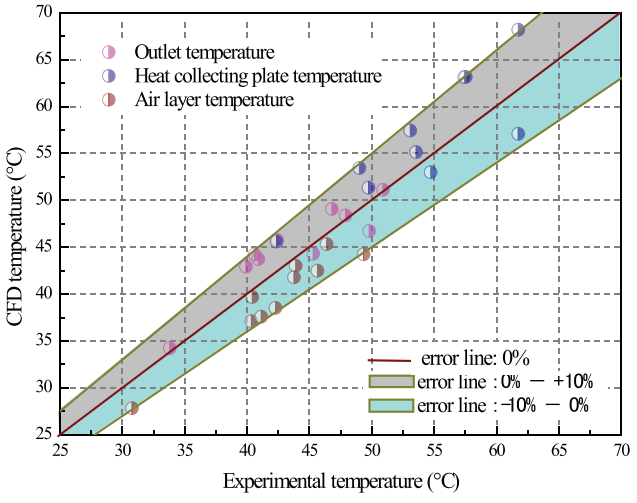


**Fig. 7** Comparison between CFD simulation output and experimental data

effect for the TSC.

The simulated contour plot for the air velocity in the air layer at different times are shown in Figure 9. The air-speed near the permeable holes quadrupled the suction speed of the outlet fan due to the jet speed at the orifice. At 11:00, the fluid in the air layer flew along the wall at the lower half-section and then along the heat-collection plate at the upper half. This occurred because a velocity gradient, which was created by the temperature difference between the collection plate and the air, was larger than the viscosity of air. Hence, the air was pushed to the wall and lifted along the wall due to the viscosity effect. On the other hand, air within the air layer quickly pushed against the heat collection plate at 12:00. This occurred because the temperature gradient was greater than the viscosity of the air, and the direction of both viscosity and temperature gradient was the same after the air had touched the collection plate. Since both the heat collection plate and the air temperature were low at 17:00, the air pushed upward and against the wall.

### 4.2 Effect of the infiltration-hole diameter and unevenness on fresh air preheating

The main factors for the heat transfer of the porous heat-collection plate are its height ratio and hole diameter. The outlet-temperature variations for the hole diameter and height ratio with time are shown in Figure 10 and Figure 11. The results are the same as the winter data, with the outlet-temperature peaking at 14. In order to ensure that the exit temperature is not lower than the target indoor-temperature of 20 °C, it is best to operate from 11:30 to 17:00. In addition, it can be found that changes in hole diameter and height ratio had little effect on the outlet temperature. However, when the hole diameter was 6 mm

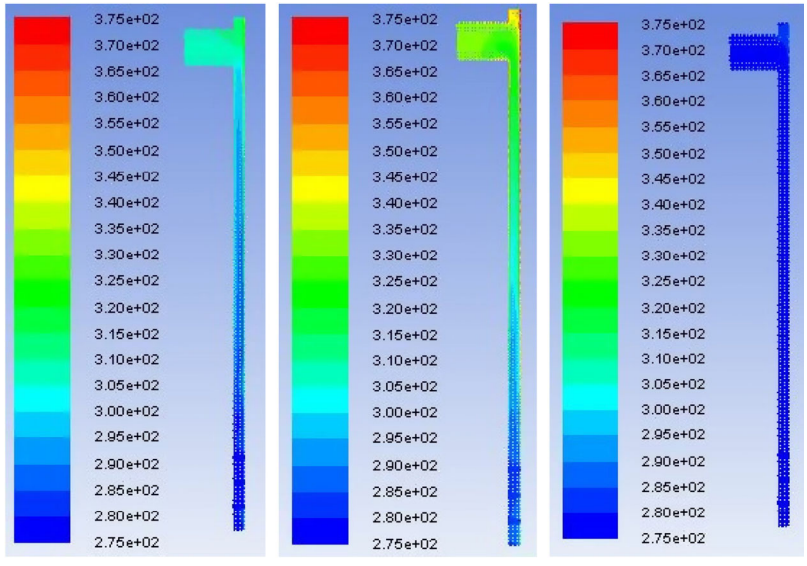


**Fig. 8** Variation of the air temperature within the air layer at different times

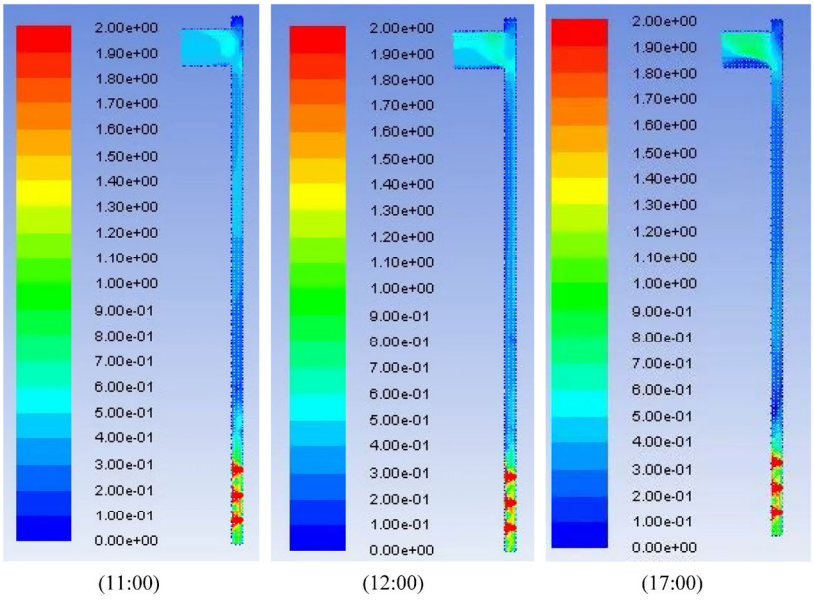


**Fig. 9** Variation of the air velocity within the air layer at different times

or the height ratio was 0.9, the outlet temperature changed about 5 °C/h compared to other design conditions. This was because, when the height was relatively high, many holes were near the fan. This produced a "short-circuit" with regard to airflow. When the hole diameter was large, the permeable air flow produced stripping, and part of the air no longer moved upward along the heat-collection plate, which reduced the heat exchange.

### 4.3 Effect of air-layer thickness on preheating of fresh air

The outlet temperature variation with time, at different air-layer thicknesses, was measured, see Figure 12. The changing air-layer thickness had a significant effect on the outlet temperature and correlated negatively. This indicates that within the allowable range of the structure, minimizing the air-layer thickness improves the heat transfer. This is because the thinner the air-layer, the more air flows through the small holes into the air layer and pushes upwards against the heat-collection plate, which was less likely to be detached, and the amount of exchanged heat increased. When the air-layer thickness was 30 mm, the response time of the system improved significantly. When the thickness of the air layer was 30 mm, the average air supply temperature

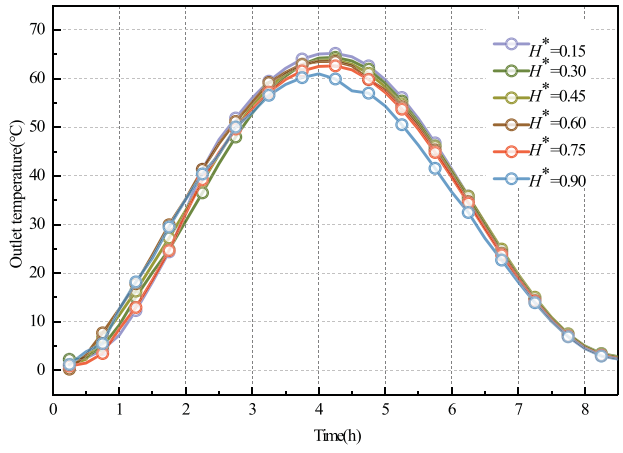


**Fig. 10** Variation of the outlet temperature with time for different height ratios ($D$ = 4mm, $\delta$ = 50mm, $v_s$ = 0.525m/s)

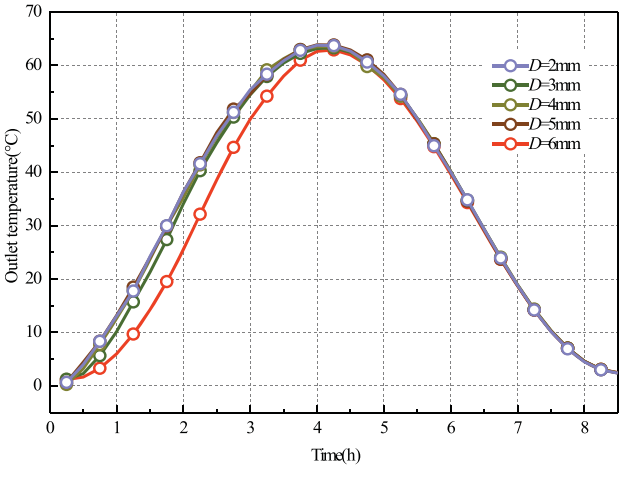


**Fig. 11** Variation of outlet temperature with time for different hole diameters ($H^*$ = 0.60, $\delta$ = 50mm, $v_s$ = 0.525m/s)

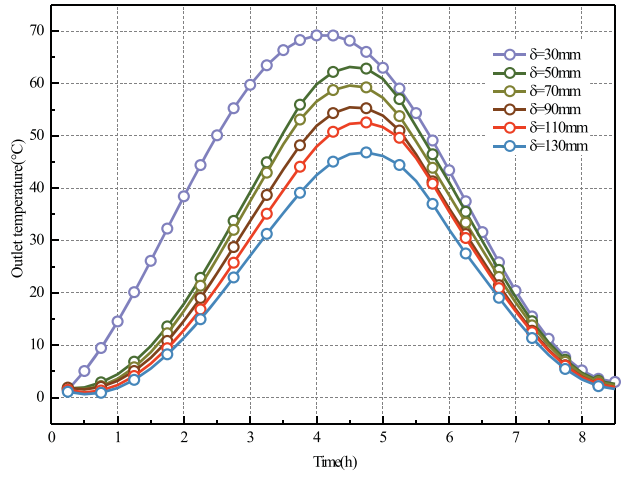


**Fig. 12** Variation of the outlet temperature with time for different air layer thicknesses ($D$ = 2mm, $H^*$ = 0.3, $v_s$ = 0.525m/s)

per hour can reach 39 °C, and the maximum could reach 70 °C. Although the outlet temperature was high, there was a significant overheating problem, so the air-layer thickness needed to be adjusted according to the requirement of the room. If the required air-supply temperature-target was greater than the suitable indoor temperature of 10 °C, then when the air-layer thickness was 50 mm, the average hourly supply air temperature was required and no overheating could occur.

### 4.4 Effect of fan suction speed on preheating of fresh air

The variation of the outlet temperature with time, at fan suction speed, is shown in Figure 13. The outlet temperature decreased as the suction speed of the fan increased. This occurs because the suction speed could increase the heat-exchange time between the air and the collection plate. In addition, the higher the suction speed, the worse was the warming effect of the fresh air, and the amplitude was reduced. The magnitude of suction speed did not affect the response time of system. Therefore, although the amplitude increased with decreasing suction speed, the trend was largely the same. It was assumed that 20 °C was the lowest temperature, which was allowed for the air supply. Furthermore, the period of time, when the air-supply temperature was above 20 °C was labeled as "usable time". As the air speed increased, the amplitude decreased, and the usable time became shorter. The operational strategy investigated in this paper means that an additional heat source was supplied via smart regulation during the period when the temperature target was not met.

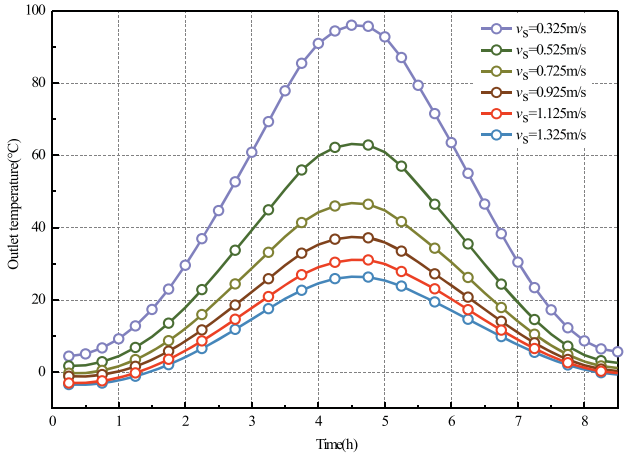


**Fig. 13** Variation of the outlet temperature with time for different fan suction speeds ($D$ = 2mm, $H^*$ = 0.3, $\delta$ = 50mm)

## 5 Discussion and analysis

### 5.1 Heat-collection efficiency and heat-exchange efficiency

As shown in Figure 14, the heat-collection efficiency was

negatively correlated with the air-layer thickness and positively correlated with the suction speed. The heat collection efficiency increased obviously with the decrease of air layer. This was different from the conclusion of Badache et al. (2013). Through comparative analysis, the reason for this difference was that the non-uniform perforation made the air flow pattern changed greatly. Under the condition of uniform perforation, the heat exchange between the air and the heat collecting plate took place mainly on the outer side heat collection plate, while the proportion of heat exchange between the inner side heat collection plate was small. The non-uniform perforation made the heat transfer of the outer heat collection plate decreased due to the heat transfer of the outer heat collection plate mainly occurred near the small holes, while the heat transfer of the inner heat collection plate greatly increased. The thickness of the air layer mainly affected the heat transfer inside the heat collection plate, so the important discovery of this paper was that the effect of the air layer thickness on the non-uniform perforation was much greater than that on the uniform perforation. However, the variation introduced by the fan suction speed was opposite to the change of the outlet temperature. This was because the increase in suction speed caused the air temperature to decrease. As a result, the temperature difference between the heat-collection plate and air became larger, and the heat exchange was increased, which, in turn, increases the heat-collection efficiency. The heat-collection efficiency reached a maximum for an air-layer thickness of 30mm and a suction speed of 1.35 m/s, i.e., 93% and 86%, respectively. The trend of the heat-collection efficiency with height ratio and hole diameter was not clear.

The heat exchange efficiency was inversely correlated with the hole diameter and height ratio because the increasing hole diameter increased the air permeation frequency, which

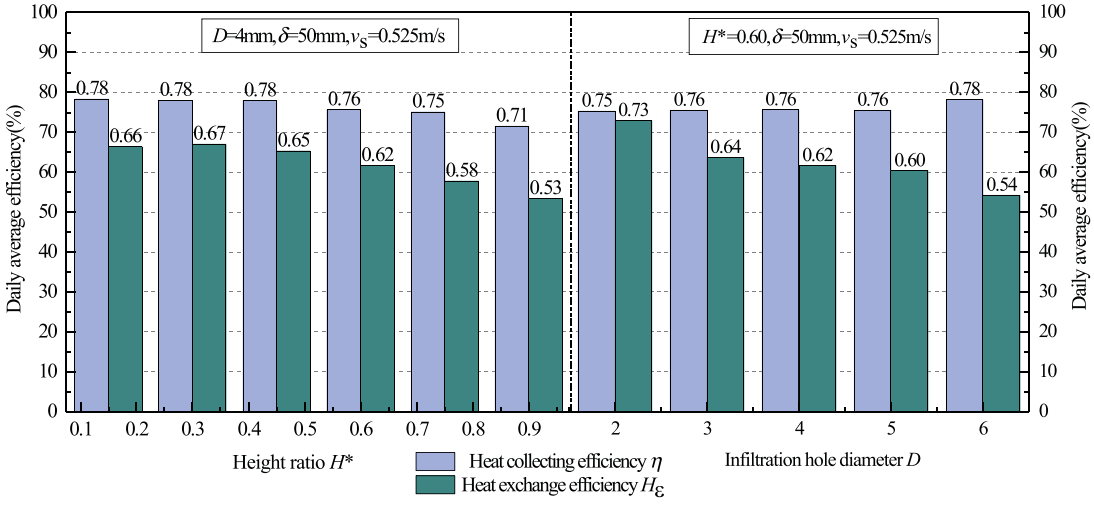


(a) Effect of height ratio and infiltration hole diameter.

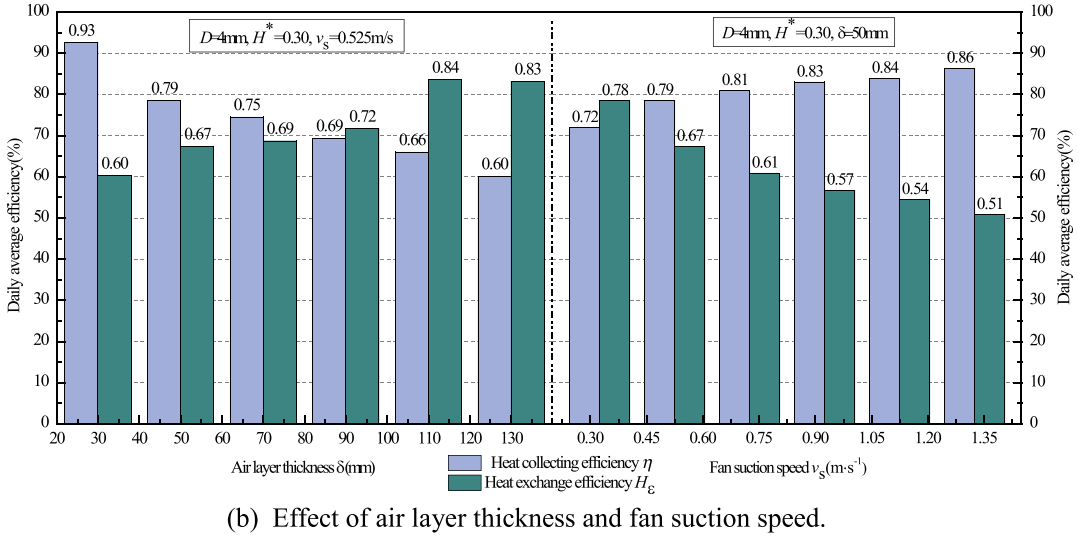


(b) Effect of air layer thickness and fan suction speed.

**Fig. 14** Heat collection efficiency and heat exchange efficiency under different conditions

makes it easier for the surface of the collection plate to form a boundary layer. The existence of the boundary layer reduced the convective heat-loss of the collector plate and the external environment. Hence, the temperature of the collector plate decreased less and the heat-exchange efficiency decreased. On the other hand, the air-layer became so thick that the amount of air, which exchanged heat with the heat-collection plate inside the TSC system, increased. This decreased the temperature of the heat-collection plate and increased the heat-exchange efficiency.

The dependency of the fitted heat-collection efficiency and heat exchange efficiency on time is shown in Figure 15. The peak occurred nearly two hours after the peak of solar radiation intensity, and the curve was similar to the ambient temperature, which suggests a positive correlation with ambient temperature.

### 5.2 Convective heat transfer of the system

The average hourly convective heat-transfer of the system was obtained using a single-factor sensitivity analysis, see Table 4. When the height ratio was 0.45, the average convective heat transfer reached the maximum (451.1 W/h). It was 27.7 W/h larger than for the non-uniform hole opening, and the average efficiency was increased by 6.5%. This result showed that the non-uniform opening can improve the convective heat-transfer and reduce the short circuit of the air flow. A sudden change occurred, when the hole diameter was 6 mm, and the convective heat-transfer decreased by more than 60 W/h. This indicated that a non-suitable hole diameter causes the separation of the boundary layer. While an increase in fan suction speed may reduce the temperature of the air outlet it may also increase the heat gain in the room. The relationship between additional heat gain and heating load would benefit from a more-detailed study.

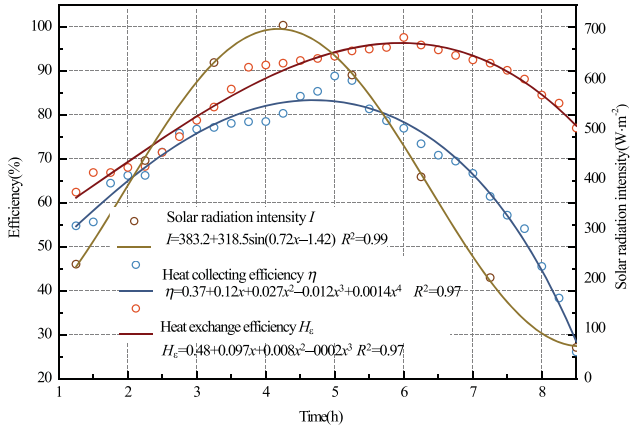


**Fig. 15** Variation of heat collection efficiency and heat exchange efficiency with time

### 5.3 Analysis of applications

Although fresh air increases the oxygen content in the room it also introduces an extra heating load, and the supply-air temperature decrease when the fresh air volume increases. According to Eq. (4), the relationship between heating load and the fresh air volume for different time periods was determined. Different buildings required different ventilation periods depending on their primary purposes/usage. Therefore, the excess heating load due to colder fresh air should also be considered. The calculation of the fresh air demand for the building was based on the same area and the same number of people (Lu 2008). After combining the existing specification data with the research results of this paper, the improvement effect of the TSC on the heating load was determined.

The relationship between fresh-air volume and TSC air-supply temperature is shown in Figure 16. The increase of fresh air volume decreases the outlet temperature, which was unavoidable and expected. However, when the fresh air volume was greater than 35 $m^3$/h, it even appeared that the average air supply for a day was lower than the target temperature of 20 °C. Also, the greater the air volume, the greater was the total heat absorbed by the collection plate. However, the TSC, a device designed to improve the indoor temperature, cannot operate independently if accompanied by a large air volume. The best solution was to add an auxiliary heat source in real time.

The relationship between fresh air volume, fresh air heating-load, and the adaptive ranges of the different buildings is shown in Figure 17. The fresh air heating-load and air volume for different time periods were mostly linear, and the air volume increased, which increased the fresh air heating-load. When using the TSC system, the fresh air heating-load was significantly reduced by an average of 476.2 W. Overall, the fresh air heating-load in the morning is greater than in the afternoon, and the afternoon heating-load is greater than the one at noon. The heat gain of the room at noon was provided by the TSC and decreased as the air volume increased. Furthermore, the school could fully meet its demand for fresh air and heat when using the TSC. Also, the office buildings could basically meet their needs, while the hotels could not meet their requirements. However, according to a previous temperature correlation study, it is known that the fresh air volume was greater than 35 $m^3$/h, which caused the "usable time" to be unavailable. As a result, the office buildings can only meet the needs using a TSC at noon.

## 6 Conclusions

The time-dependent thermal characteristics of transpired

**Table 4** Convective heat-transfer under different working conditions

| Type | Operation parameters | Value | Average convection heat transfer (W) | Fresh air volume ($m^3 \cdot h^{-1}$) |
|---|---|---|---|---|
| Hole diameter $D$=4mm<br>Fan suction speed $v_s$=0.525m/s<br>Air-layer thickness $\delta$=50mm | Height ratio $H^*$ | 0.15 | 411.6 | 33.4 |
| | | 0.30 | 403.9 | |
| | | 0.45 | 451.1 | |
| | | 0.60 | 447.1 | |
| | | 0.75 | 400.6 | |
| | | 0.90 | 423.4 | |
| Air-layer thickness $\delta$=50mm<br>Height ratio $H^*$=0.6<br>Fan suction speed $v_s$=0.525m/s | Hole diameter $D$ (mm) | 2 | 447.6 | 33.4 |
| | | 3 | 447.1 | |
| | | 4 | 446.9 | |
| | | 5 | 444.6 | |
| | | 6 | 383.4 | |
| Height ratio $H^*$=0.3<br>Hole diameter $D$=2mm<br>Fan suction speed $v_s$=0.525m/s | Air-layer thickness $\delta$ (mm) | 30 | 470.9 | 33.4 |
| | | 50 | 363.4 | |
| | | 70 | 345.1 | |
| | | 90 | 319.8 | |
| | | 110 | 302.0 | |
| | | 130 | 272.4 | |
| Air-layer thickness $\delta$=50mm<br>Height ratio $H^*$=0.6<br>Hole diameter $D$=4mm | Fan suction speed $v_s$ ($m \cdot s^{-1}$) | 0.325 | 329.9 | 20.7 |
| | | 0.525 | 363.4 | 33.4 |
| | | 0.725 | 363.5 | 46.1 |
| | | 0.925 | 387.6 | 58.8 |
| | | 1.125 | 398.3 | 71.6 |
| | | 1.325 | 404.3 | 84.3 |

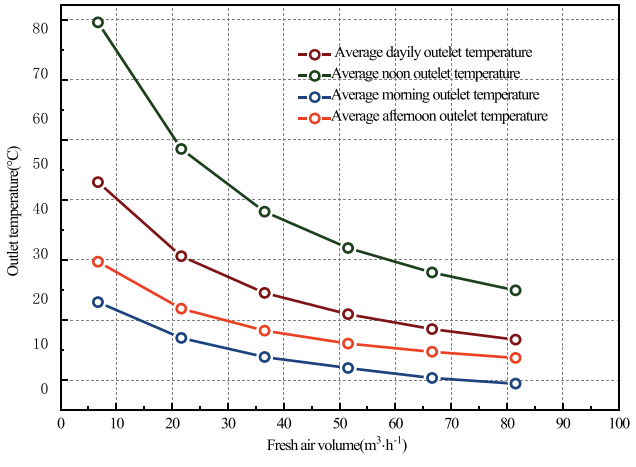


**Fig. 16** Outlet temperature as a function of fresh airflow

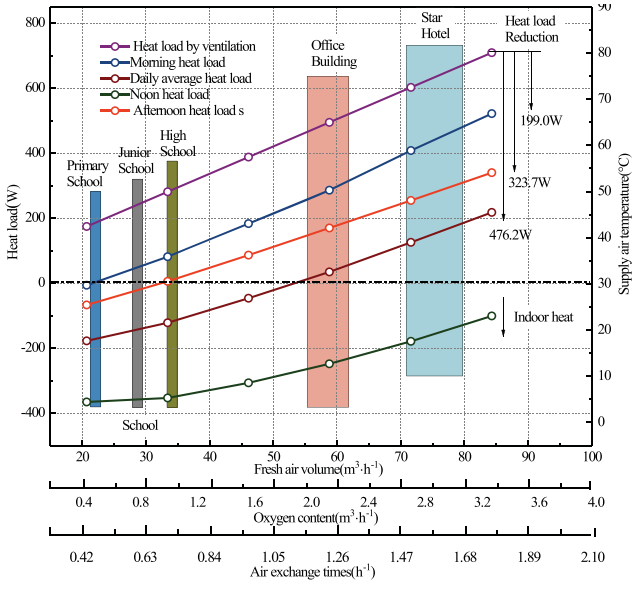


**Fig. 17** Average fresh air heating-load and supply air temperature vs. fresh airflow for five different buildings (oxygen content and air-exchange times are also shown)

solar collector operation were studied via numerical simulation. The effect of the system design on the thermal efficiency was determined using single-factor sensitivity analysis. In addition, the convective heat-transfer and fresh-air volume of the system were combined with realistic conditions. The

following conclusions can be summarized:

(1) A non-uniform opening can increase the convective heat-transfer by about 6.5% compared to a uniform opening. A suitably chosen height ratio can increase the convective heat transfer, and the convective heat transfer was largest when the height ratio was 0.45.

(2) Even though the hole-diameter hardly affected the outlet temperature, when the hole diameter exceeded 6 mm, the outlet temperature dropped suddenly by nearly 8 °C. Therefore, a carefully chosen range for the hole diameter is essential for effective heat transfer in the system.

(3) The air-layer thickness has a strong effect on the heat-collection efficiency of the system. The heat-collection efficiency increases with decreasing air-layer thickness, and the maximum reached 93%. The effect of the air layer thickness on the non-uniform perforation was much greater than that on the uniform perforation.

(4) Although a higher air-speed can improve heat transfer, it can also reduce the usable time and outlet temperature. In addition, with increasing fresh air volume, the reduction rate of the fresh air heating-load is lower than its rate of increase. This means that the fresh air heating-load continues to increase.

(5) The TSC can effectively reduce the fresh air heat load, with an average of about 476.2 W per day. This means TSCs are promising candidates for implementation in buildings. TSCs works best for schools, moderately well for office buildings, and poorly for hotels. Since TSCs cannot fully meet the temperature requirements, auxiliary heat-sources are usually needed. The simulation results of this paper have been confirmed by experiments. The results of this paper may be helpful for future applications and the production of improved TSCs.

## Acknowledgements

This study was supported by the National Key Research and Development Program (No. 2016YFC0700400), the National Natural Science Foundation of China (No. 51678468), and the key research and development program of Shaanxi Province, China (2018ZDCXL-SF-03-01).

## References

Badache M, Rousse DR, Hallé S, Quesada G (2013). Experimental and numerical simulation of a two-dimensional unglazed transpired solar air collector. *Solar Energy*, 93: 209–219.

Belusko M, Saman W, Bruno F (2008). Performance of jet impingement in unglazed air collectors. *Solar Energy*, 82: 389–398.

Chan HY, Zhu J, Riffat S (2013). Heat transfer analysis of the transpired solar facade. *Energy Procedia*, 42: 123–132.

Chan HY, Zhu J, Ruslan MH, Sopian K, Riffat S (2014). Thermal analysis of flat and transpired solar facades. *Energy Procedia*, 48: 1345–1354.

Chen C, Liu YF, Wang DJ (2016). The optimization and adaptation analysis on the Insulation structure of the Trombe wall. *Journal of Solar Energy*, 37: 2889–2895. (in Chinese)

Chen QZ (2010). Application research of passive solar building with phase change wallboard in Shenyang area. PhD Thesis, Chongqing University, China. (in Chinese)

Choudhary R, Augenbroe G, Gentry R, Hu H (2008). Simulation-enhanced prototyping of an experimental solar house. *Building Simulation*, 1: 336–355.

Collins MR, Abulkhair H (2014). An evaluation of heat transfer and effectiveness for unglazed transpired solar air heaters. *Solar Energy*, 99: 231–245.

Croitoru CV, Nastase I, Bode FI, Meslem A (2016). Thermodynamic investigation on an innovative unglazed transpired solar collector. *Solar Energy*, 131: 21–29.

van Decker GWE, Hollands KGT, Brunger AP (2001). Heat-exchange relations for unglazed transpired solar collectors with circular holes on a square or triangular pitch. *Solar Energy*, 71: 33–45.

Dymond CS, Kutscher CF (1995). A computer design model for transpired solar collector systems. In: Proceedings of the ASME/JSME/JSES International Solar Energy Conference, American Society of Mechanical Engineers, New York, USA.

Gao M, Wang D, Liu Y, Wang Y, Zhou Y (2020). A study on thermal performance of a novel glazed transpired solar collector with perforating corrugated plate. *Journal of Cleaner Production*, 257: 120443.

Gawlik K, Christensen C, Kutscher C (2005). A numerical and experimental investigation of low-conductivity unglazed, transpired solar air heaters. *Journal of Solar Energy Engineering*, 127: 153–155.

Gholampour M, Ameri M (2014). Design considerations of unglazed transpired collectors: energetic and exergetic studies. *Journal of Solar Energy Engineering*, 136(3): 031004.

He W, Wang C, Ji J (2016). Study on the effect of Trombe wall with venetian blind structure on indoor temperature in different blade angle. *Acta Energiae Solaris Sinica*, 37: 673–677. (in Chinese)

Helenice MS, Luis B, Manuela A, Rosana C (2011). Trombe wall thermal performance for a modular façade system in different portuguese climates: lisbon, porto, lajes and funchal. In: Proceedings of the 12th International IBPSA Building Simulation Conference, Sydney, Australia.

Hong S, He G, Ge W, Wu Q, Lv D, Li Z (2019). Annual energy performance simulation of solar chimney in a cold winter and hot summer climate. *Building Simulation*, 12: 847–856.

Kutscher CF, Christensen CB, Barker GM (1993). Unglazed transpired solar collectors: Heat loss theory. *Journal of Solar Energy Engineering*, 115: 182–188.

Li Y, Duanmu X, Sun Y, Li J, Jia H (2007). Study on the air movement character in solar wall system. In: Proceedings of the 10th International IBPSA Building Simulation Conference, Beijing China.

Li S, Karava P, Savory E, Lin WE (2013). Airflow and thermal analysis of flat and corrugated unglazed transpired solar collectors. *Solar Energy*, 91: 297–315.

Liu Y, Li Z (2015). Research on passive solar energy utilization building technology. *Urban Construction Theory Research: Electronic Edition*, 5(31): 2167–2168. (in Chinese)

Liu X, Zhou Y, Zhang G (2018). Numerical study on cooling performance of a ventilated Trombe wall with phase change materials. *Building Simulation*, 11: 677–694.

Liu Y, Zhou Y, Chen Y, Wang D, Wang Y, Zhu Y (2020). Comparison of support vector machine and copula-based nonlinear quantile regression for estimating the daily diffuse solar radiation: A case study in China. *Renewable Energy*, 146: 1101–1112.

Lu Y (2008). Practical Air Conditioning Heating Design Manual. Beijing: China Architecture & Building Press. (in Chinese)

Motahar S (2010). An analysis of unglazed transpired solar collectors based on exergetic performance criteria. *International Journal of Thermodynamics*, 13: 153–160.

Njomo D (2000). Unglazed selective absorber solar air collector: Heat exchange analysis. *Heat and Mass Transfer*, 36: 313–317.

Rad HM, Ameri M (2016). Energy and exergy study of unglazed transpired collector-2stage. *Solar Energy*, 132: 570–586.

Safer N, Woloszyn M, Roux JJ (2005). Three-dimensional simulation with a CFD tool of the airflow phenomena in single floor double-skin facade equipped with a venetian blind. *Solar Energy*, 79: 193–203.

Sameti M, Kasaeian A (2015). Numerical simulation of combined solar passive heating and radiative cooling for a building. *Building Simulation*, 8: 239–253.

Saxena A, Varun, El-Sebaii AA (2015). A thermodynamic review of solar air heaters. *Renewable and Sustainable Energy Reviews*, 43: 863–890.

Torcellini P, Pless S (2004). Trombe Walls in low-energy buildings: Practical experiences. Paper presented at the World Renewable Energy Congress VIII and Expo, Denver, CO, USA.

Wang YF (2009). Research on the thermal performance of the solar wall system. Master Thesis, Harbin Institute of Technology, China. (in Chinese)

Wang W, Tian Z, Ding Y (2013). Investigation on the influencing factors of energy consumption and thermal comfort for a passive solar house with water thermal storage wall. *Energy and Buildings*, 64: 218–223.

Wang D, Gao Q, Liu Y, Wang Y, Chen Y, Liu Y, Liu J (2019). Experimental study on heating characteristics and parameter optimization of transpired solar collectors. *Applied Energy*, 238: 534–546.

Zhang Z, Xiang S, Zhang Y, Wu A, Cai L, Guo G, Huang J (2006). A new type of hybrid magnetic semiconductor based upon polymeric iodoplumbate and metal–organic complexes as templates. *Inorganic Chemistry*, 45: 1972–1977.

Zhang Y (2008). Study of urban sewage heat energy utilization and its application. Master Thesis, Jilin University, China. (in Chinese)